



Search for proton decay via $p \rightarrow e^+\pi^0$ and $p \rightarrow \mu^+\pi^0$ in 0.31 megaton \cdot years exposure of the Super-Kamiokande water Cherenkov detector

K. Abe,^{1,31} Y. Haga,¹ Y. Hayato,^{1,31} M. Ikeda,¹ K. Iyogi,¹ J. Kameda,^{1,31} Y. Kishimoto,^{1,31} M. Miura,^{1,31} S. Moriyama,^{1,31}
M. Nakahata,^{1,31} T. Nakajima,¹ Y. Nakano,¹ S. Nakayama,^{1,31} A. Orii,¹ H. Sekiya,^{1,31} M. Shiozawa,^{1,31} A. Takeda,^{1,31}
H. Tanaka,¹ T. Tomura,^{1,31} R. A. Wendell,^{1,31} R. Akutsu,² T. Irvine,² T. Kajita,^{2,31} K. Kaneyuki,^{2,31,*} Y. Nishimura,²
E. Richard,² K. Okumura,^{2,31} L. Labarga,³ P. Fernandez,³ J. Gustafson,⁴ C. Kachulis,⁴ E. Kearns,^{4,31} J. L. Raaf,⁴
J. L. Stone,^{4,31} L. R. Sulak,⁴ S. Berkman,⁵ C. M. Nantais,⁵ H. A. Tanaka,⁵ S. Tobayama,⁵ M. Goldhaber,^{6,*}
W. R. Kropp,⁷ S. Mine,⁷ P. Weatherly,⁷ M. B. Smy,^{7,31} H. W. Sobel,^{7,31} V. Takhistov,⁷ K. S. Ganezer,⁸ B. L. Hartfiel,⁸
J. Hill,⁸ N. Hong,⁹ J. Y. Kim,⁹ I. T. Lim,⁹ R. G. Park,⁹ A. Himmel,¹⁰ Z. Li,¹⁰ E. O'Sullivan,¹⁰ K. Scholberg,^{10,31}
C. W. Walter,^{10,31} T. Wongjirad,¹⁰ T. Ishizuka,¹¹ S. Tasaka,¹² J. S. Jang,¹³ J. G. Learned,¹⁴ S. Matsuno,¹⁴ S. N. Smith,¹⁴
M. Friend,¹⁵ T. Hasegawa,¹⁵ T. Ishida,¹⁵ T. Ishii,¹⁵ T. Kobayashi,¹⁵ T. Nakadaira,¹⁵ K. Nakamura,^{15,31} Y. Oyama,¹⁵
K. Sakashita,¹⁵ T. Sekiguchi,¹⁵ T. Tsukamoto,¹⁵ A. T. Suzuki,¹⁶ Y. Takeuchi,^{16,31} T. Yano,¹⁶ S. V. Cao,¹⁷ T. Hiraki,¹⁷
S. Hirota,¹⁷ K. Huang,¹⁷ T. Kikawa,¹⁷ A. Minamino,¹⁷ T. Nakaya,^{17,31} K. Suzuki,¹⁷ Y. Fukuda,¹⁸ K. Choi,¹⁹
Y. Itow,¹⁹ T. Suzuki,¹⁹ P. Mijakowski,²⁰ K. Frankiewicz,²⁰ J. Hignight,²¹ J. Imber,²¹ C. K. Jung,²¹ X. Li,²¹
J. L. Palomino,²¹ M. J. Wilking,²¹ C. Yanagisawa,^{21,†} D. Fukuda,²² H. Ishino,²² T. Kayano,²² A. Kibayashi,²²
Y. Koshio,²² T. Mori,²² M. Sakuda,²² C. Xu,²² Y. Kuno,²³ R. Tacik,^{24,33} S. B. Kim,²⁵ H. Okazawa,²⁶ Y. Choi,²⁷
K. Nishijima,²⁸ M. Koshihara,²⁹ Y. Totsuka,^{29,*} Y. Suda,³⁰ M. Yokoyama,^{30,31} C. Bronner,³¹ M. Hartz,³¹ K. Martens,³¹
Ll. Marti,³¹ Y. Suzuki,³¹ M. R. Vagins,^{31,‡} J. F. Martin,³² A. Konaka,³³ S. Chen,³⁴ Y. Zhang,³⁴ and R. J. Wilkes³⁵

(Super-Kamiokande Collaboration)

¹*Kamioka Observatory, Institute for Cosmic Ray Research, University of Tokyo,
Kamioka, Gifu 506-1205, Japan*

²*Research Center for Cosmic Neutrinos, Institute for Cosmic Ray Research,
University of Tokyo, Kashiwa, Chiba 277-8582, Japan*

³*Department of Theoretical Physics, University Autonoma Madrid, 28049 Madrid, Spain*

⁴*Department of Physics, Boston University, Boston, Massachusetts 02215, USA*

⁵*Department of Physics and Astronomy, University of British Columbia,
Vancouver, British Columbia V6T1Z4, Canada*

⁶*Physics Department, Brookhaven National Laboratory, Upton, New York 11973, USA*

⁷*Department of Physics and Astronomy, University of California,
Irvine, Irvine, California 92697-4575, USA*

⁸*Department of Physics, California State University, Dominguez Hills, Carson, California 90747, USA*

⁹*Department of Physics, Chonnam National University, Kwangju 500-757, Korea*

¹⁰*Department of Physics, Duke University, Durham North Carolina 27708, USA*

¹¹*Junior College, Fukuoka Institute of Technology, Fukuoka, Fukuoka 811-0295, Japan*

¹²*Department of Physics, Gifu University, Gifu, Gifu 501-1193, Japan*

¹³*GIST College, Gwangju Institute of Science and Technology, Gwangju 500-712, Korea*

¹⁴*Department of Physics and Astronomy, University of Hawaii, Honolulu, Hawaii 96822, USA*

¹⁵*High Energy Accelerator Research Organization (KEK), Tsukuba, Ibaraki 305-0801, Japan*

¹⁶*Department of Physics, Kobe University, Kobe, Hyogo 657-8501, Japan*

¹⁷*Department of Physics, Kyoto University, Kyoto, Kyoto 606-8502, Japan*

¹⁸*Department of Physics, Miyagi University of Education, Sendai, Miyagi 980-0845, Japan*

¹⁹*Solar Terrestrial Environment Laboratory, Nagoya University, Nagoya, Aichi 464-8602, Japan*

²⁰*National Centre For Nuclear Research, 00-681 Warsaw, Poland*

²¹*Department of Physics and Astronomy, State University of New York at Stony Brook,
New York 11794-3800, USA*

²²*Department of Physics, Okayama University, Okayama, Okayama 700-8530, Japan*

²³*Department of Physics, Osaka University, Toyonaka, Osaka 560-0043, Japan*

²⁴*Department of Physics, University of Regina, 3737 Wascana Parkway, Regina SK S4S0A2, Canada*

²⁵*Department of Physics, Seoul National University, Seoul 151-742, Korea*

²⁶*Department of Informatics in Social Welfare, Shizuoka University of Welfare,
Yaizu, Shizuoka 425-8611, Japan*

²⁷*Department of Physics, Sungkyunkwan University, Suwon 440-746, Korea*

²⁸*Department of Physics, Tokai University, Hiratsuka, Kanagawa 259-1292, Japan*²⁹*The University of Tokyo, Bunkyo, Tokyo 113-0033, Japan*³⁰*Department of Physics, University of Tokyo, Bunkyo, Tokyo 113-0033, Japan*³¹*Kavli Institute for the Physics and Mathematics of the Universe (WPI), The University of Tokyo Institutes for Advanced Study, University of Tokyo, Kashiwa, Chiba 277-8583, Japan*³²*Department of Physics, University of Toronto, 60 St., Toronto, Ontario M5S1A7, Canada*³³*TRIUMF, 4004 Wesbrook Mall, Vancouver, British Columbia V6T2A3, Canada*³⁴*Department of Engineering Physics, Tsinghua University, Beijing 100084, China*³⁵*Department of Physics, University of Washington, Seattle, Washington 98195-1560, USA*

(Received 13 October 2016; published 6 January 2017)

We have searched for proton decay via $p \rightarrow e^+\pi^0$ and $p \rightarrow \mu^+\pi^0$ using Super-Kamiokande data from April 1996 to March 2015, 0.306 megaton · years exposure in total. The atmospheric neutrino background rate in Super-Kamiokande IV is reduced to almost half that of phase I-III by tagging neutrons associated with neutrino interactions. The reach of the proton lifetime is further enhanced by introducing new signal criteria that select the decay of a proton in a hydrogen atom. No candidates were seen in the $p \rightarrow e^+\pi^0$ search. Two candidates that passed all of the selection criteria for $p \rightarrow \mu^+\pi^0$ have been observed, but these are consistent with the expected number of background events of 0.87. Lower limits on the proton lifetime are set at $\tau/B(p \rightarrow e^+\pi^0) > 1.6 \times 10^{34}$ years and $\tau/B(p \rightarrow \mu^+\pi^0) > 7.7 \times 10^{33}$ years at 90% confidence level.

DOI: 10.1103/PhysRevD.95.012004

I. INTRODUCTION

Grand unified theories (GUTs) [1] are motivated by the apparent convergence of the running couplings of the strong, weak, and electromagnetic forces at high energy (10^{15} – 10^{16} GeV). Such a high energy scale is out of the reach of accelerators; however, a general feature of GUTs is their prediction of the instability of protons by baryon number violating decays. The grand unification idea is successful in many aspects; these include an understanding of electric charge quantization, the coexistence of quarks and leptons and their quantum numbers, and as an explanation of the scale of the neutrino masses. Proton decay now remains as a key missing piece of evidence for grand unification [2].

In GUTs, nucleon decay can proceed via exchange of a massive gauge boson between two quarks. The favored gauge-mediated decay mode in many GUTs is $p \rightarrow e^+\pi^0$. On the other hand, the flipped $SU(5)$ GUT model [3] predicts that the $p \rightarrow \mu^+\pi^0$ mode can have a branching ratio comparable to that of the $p \rightarrow e^+\pi^0$ mode. Water Cherenkov detectors are suitable for these decay modes because all final state particles after the proton decay are detectable since they are above the Cherenkov threshold, enabling reconstruction of the proton mass and momentum to distinguish these events from atmospheric neutrino backgrounds. The dominant inefficiency comes from Fermi momentum of protons and pion interactions inside the nucleus, which distorts the reconstructed proton mass

and momentum distributions. However, the two hydrogen atoms in a water molecule are outside of the oxygen nucleus; these act as free protons which are not subject to the nuclear effects. As a result, water Cherenkov detectors can achieve high efficiency for $p \rightarrow e^+\pi^0$ and $p \rightarrow \mu^+\pi^0$ searches.

In the minimal $SU(5)$ GUT [4], the predicted proton lifetime to $e^+\pi^0$ is $10^{31\pm 1}$ years, which has been ruled out by experimental results from IMB [5], Kamiokande [6], and Super-Kamiokande [7–9]. However, longer lifetimes for this decay mode ($\sim 10^{35}$ years) are predicted by other classes of GUTs e.g., minimal SUSY $SU(5)$ [10], flipped $SU(5)$ [3], $SO(10)$ [11], etc., which are subject to experimental tests. The experimental searches for the gauge-mediated proton decays are further motivated by the discovery of a Higgs-like boson with a mass around $125 \text{ GeV}/c^2$ [12,13]. This paper describes the search for $p \rightarrow e^+\pi^0$ and $p \rightarrow \mu^+\pi^0$ by improved analysis techniques with 0.306 megaton · years of Super-Kamiokande data.

II. SUPER-KAMIOKANDE DETECTOR

Super-Kamiokande (SK) is a large upright cylindrical water Cherenkov detector, 39 m in diameter and 41 m in height, containing 50 ktons of pure water. Details of the detector have been described in Ref. [14]. The previous publication of $p \rightarrow e^+\pi^0$ and $p \rightarrow \mu^+\pi^0$ limits [9] reported results using 220 kiloton · years exposure with 90% confidence level lower limits on the proton lifetime set at 1.3×10^{34} and 1.1×10^{34} years, respectively. In the SK-I period, the photocathode coverage inside the inner detector was 40%; this was reduced to 19% during SK-II. After

*Deceased.

†Also at BMCC/CUNY, Science Department, New York, New York, USA.

production and installation of replacement 50-cm photo-multiplier tubes (PMTs), the photocathode coverage inside the detector was recovered to the original 40% in 2006. The period between July 2006 and September 2008 is defined as SK-III. In the summer of 2008, the detector readout electronics were upgraded with improved performance, including a “deadtime free” data acquisition system that records all successive PMT hit information [15]. This has been the configuration of the detector since September 2008; it is called SK-IV. The new configuration of the detector contributes to improved tagging efficiency of Michel decay electrons in SK-IV. The tagging efficiency of Michel electrons is estimated to be 99% for SK-IV and 82% for the period before SK-IV by using $p \rightarrow \mu^+ \pi^0$ MC samples. It also enables tagging of neutrons in SK-IV. The signature of the neutron, 2.2 MeV gamma ray emission from the neutron capture on hydrogen with a mean capture time of 200 μ sec is too faint to be triggered by the data acquisition system used in SK-I through SK-III. The upgraded electronics in SK-IV adopt a triggerless readout scheme to record every hit, including all hits by 2.2 MeV gamma rays. A software trigger is then issued after every fully contained event to save all hits within a 500 μ sec timing window for physics analyses. In this paper, we use data from April 1996 up to March 2015, corresponding to 4973 live days or 306.3 kton \cdot years in total by summing up 91.7, 49.2, 31.9, 133.5 kton \cdot years of SK-I, II, III, and IV data.

III. NEUTRON TAGGING

Neutron tagging can benefit proton decay analyses, providing an additional handle for rejecting the atmospheric neutrino interactions that are the main background to proton decays. Atmospheric neutrino interactions are often accompanied by neutrons, while the probability of a neutron being emitted by deexcitation of a nucleus after proton decay is rather small, and no neutron is produced in the decay of a free proton. Furthermore, these proton decay modes do not produce neutrons in secondary interactions in water because the final state particles in these decay modes are lepton and gammas. The neutron tagging algorithm was originally developed to identify antineutrino interactions, in which a neutron is often emitted; the supernova relic neutrino search [16], the cosmic-ray-muon spallation background measurement [17], and the neutrino oscillation analysis [18] have been improved by this technique. To find 2.2 MeV γ candidates, we search for hit clusters with ≥ 7 hits within a 10 ns sliding time window, after time-of-flight (TOF) subtraction using the vertex of the prompt neutrino interaction. Sixteen variables described in Ref. [18] are input to a neural network to distinguish the 2.2 MeV γ signal from background. The efficiency of neutron tagging by this method is estimated to be $20.5 \pm 2.1\%$ with a mistagging probability of 1.8%. The performance of the neutron tagging was confirmed by

introducing a neutron source (americium-beryllium) into the SK tank [16].

IV. SIMULATION

Our simulation of the atmospheric neutrino cross sections and flux is modeled by NEUT [19] and HKKM [20]. In the case of atmospheric neutrino interactions, neutrons are generated in primary interactions (10%), hadron and meson interactions in the nucleus (17%), and interactions of hadrons in water (73%). For hadron-water interactions at energies below 3.5 GeV, our simulation uses the Nucleon-Meson-Transport-Code (NMTC), which is based on the Bertini intranuclear hadronic cascade model [21]. For low energy (< 20 MeV) neutron propagation, the Monte Carlo Ionization Chamber Analysis Package (MICAP) code [22] is employed. Thermalized neutrons are then simulated until capture on hydrogen and emission of 2.2 MeV γ -rays. Neutrons can also be generated via the deexcitation process and muon capture in water. These are not taken into account in our atmospheric neutrino simulation, but are instead included in our uncertainty by comparison of data and atmospheric ν Monte Carlo. In order to include all possible low energy backgrounds, real data taken by a random trigger are added into the simulated neutron data.

The proton decay simulation has been updated since the previous paper [23] by implementation of proton and neutron emission at deexcitation from s-state [24], and 7.5% of $p \rightarrow e^+ \pi^0$ events in oxygen are accompanied by a neutron.

A π^0 produced by bound proton decay interacts via the strong interaction and there is a significant probability of reinteraction within the nucleus prior to escape. NEUT also simulates the pion final state interactions (π -FSI). The NEUT π -FSI model is a microscopic cascade where the pion is propagated classically through the nuclear medium in finite steps; it is capable of simulating various nuclei. The π -FSI model has been tuned to various π^\pm -nucleus experimental data including C, O, Al, Fe, and has been updated [25] since the previous paper [9]. The left panel in Fig. 1 shows the π^+ cross sections of the external data and MC on ^{12}C [26], which has the largest number of data points. After tuning, the estimated rates of neutral pion absorption and charge exchange have increased around 500 MeV/c, which affects the distribution of the number of rings and causes a 5% reduction of estimated signal efficiency. Large angle scattering in the nucleus has also increased, which modifies the reconstructed proton mass and momentum distributions, resulting in a 7% reduction in estimated selection efficiency for $p \rightarrow e^+ \pi^0$ and $p \rightarrow \mu^+ \pi^0$. The right panel of Fig. 1 shows the fraction of π^0 interactions as a function of the pion momentum after the tune. The same plot for the previous simulation can be found in [27].

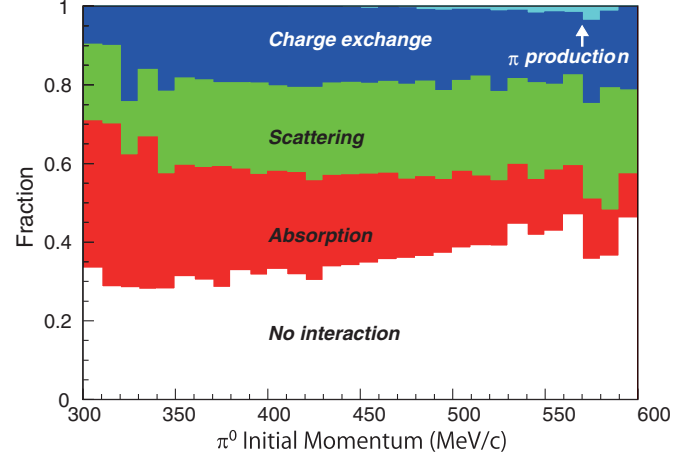
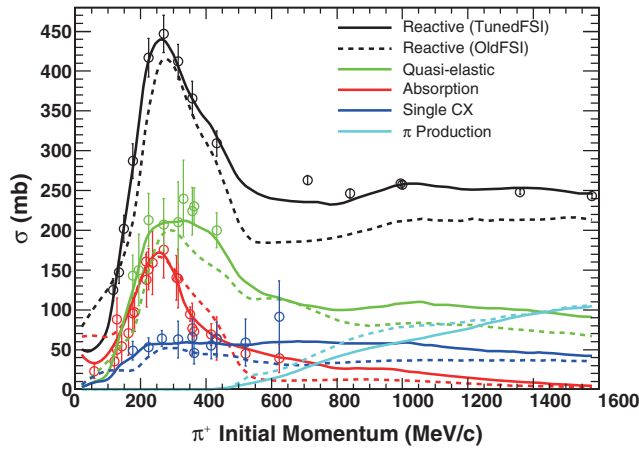


FIG. 1. The left panel shows π^+ cross sections on ^{12}C as a function of momentum. Open circles indicate existing data [26], solid and dashed lines show after and before the tune, respectively. The colors correspond to the total cross section and exclusive channels: total (black), elastic scattering (green), absorption (red), charge exchange (blue), and π production (light blue). The right panel shows cumulative fractions of neutral pion final state interactions as a function of momentum generated by $p \rightarrow e^+\pi^0$ MC. The fractions of events that undergo charge exchange, multiple π production, scattering, and absorption are shown by the various shades as labeled. Neutral pions that exit the nucleus without experiencing any final state interactions are indicated by the portion labeled “No interaction.”

V. SELECTION CRITERIA

The following cuts are applied to signal MC, atmospheric ν MC, and data:

- (Cut-1) events must be fully contained in the inner detector with the vertex position within the fiducial volume, which is defined as 2 meters inward from the detector walls (FCFV),
- (Cut-2) there must be 2 or 3 Cherenkov rings,
- (Cut-3) all rings must be electronlike for $p \rightarrow e^+\pi^0$ and one ring must be μ -like for $p \rightarrow \mu^+\pi^0$,
- (Cut-4) there must be no Michel electrons for $p \rightarrow e^+\pi^0$ and one electron for $p \rightarrow \mu^+\pi^0$,
- (Cut-5) reconstructed π^0 mass should be $85 < M_{\pi^0} < 185 \text{ MeV}/c^2$ for 3 ring events,
- (Cut-6) reconstructed total mass should be $800 < M_{\text{tot}} < 1050 \text{ MeV}/c^2$ and reconstructed total momentum P_{tot} should be less than $250 \text{ MeV}/c$,

and for SK-IV only,

- (Cut-7) there must be no tagged neutrons.

After (Cut-1), 41k FCFV events remain in data for the entire period. The events which contain two rings are allowed in (Cut-2) because one gamma ray from π^0 may fail to reconstruct if the opening angle of the two gammas is small, or the energy of the gamma is small. The fraction of 2- and 3-ring events in $p \rightarrow e^+\pi^0$ MC before (Cut-5) are 45% and 55%, respectively. The requirement (Cut-7) rejects about 50% of the background but reduces selection efficiency by 3%, in which both true and fake neutrons contribute. Figure 2 shows the number of tagged neutrons for $p \rightarrow e^+\pi^0$ (upper) and $p \rightarrow \mu^+\pi^0$ (lower) after applying (Cut-1) through (Cut-5), excluding the signal region defined by (Cut-6). These figures show that the neutron multiplicity in the atmospheric neutrino MC (solid histogram) agrees well

with data (dots). The dashed histograms show the true number of captured neutrons in the MC, indicating that additional background rejection can be achieved if the neutron tagging efficiency is improved in the future when gadolinium is dissolved in the SK water [28].

A new analysis technique [29] is applied in this paper. The signal region defined by (Cut-6) is divided into two regions: $P_{\text{tot}} < 100 \text{ MeV}/c$ and $100 \leq P_{\text{tot}} < 250 \text{ MeV}/c$. The region below $100 \text{ MeV}/c$ is dominated

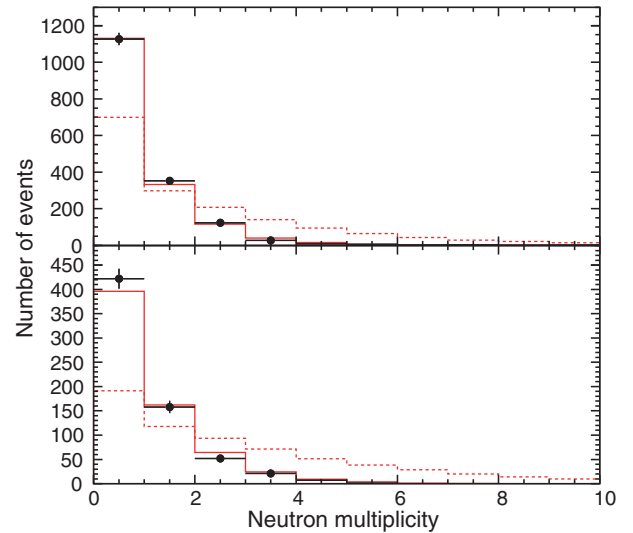


FIG. 2. Distribution of the number of tagged neutrons for $p \rightarrow e^+\pi^0$ (top) and $p \rightarrow \mu^+\pi^0$ (bottom) after applying (Cut-1) through (Cut-5), excluding the signal region defined by (Cut-6). Dots show SK-IV data with 133.5 kton \cdot years exposure, the solid histogram shows the multiplicity of tagged neutrons per event in the atmospheric ν MC, and the dashed histogram shows the true multiplicity of neutrons per event.

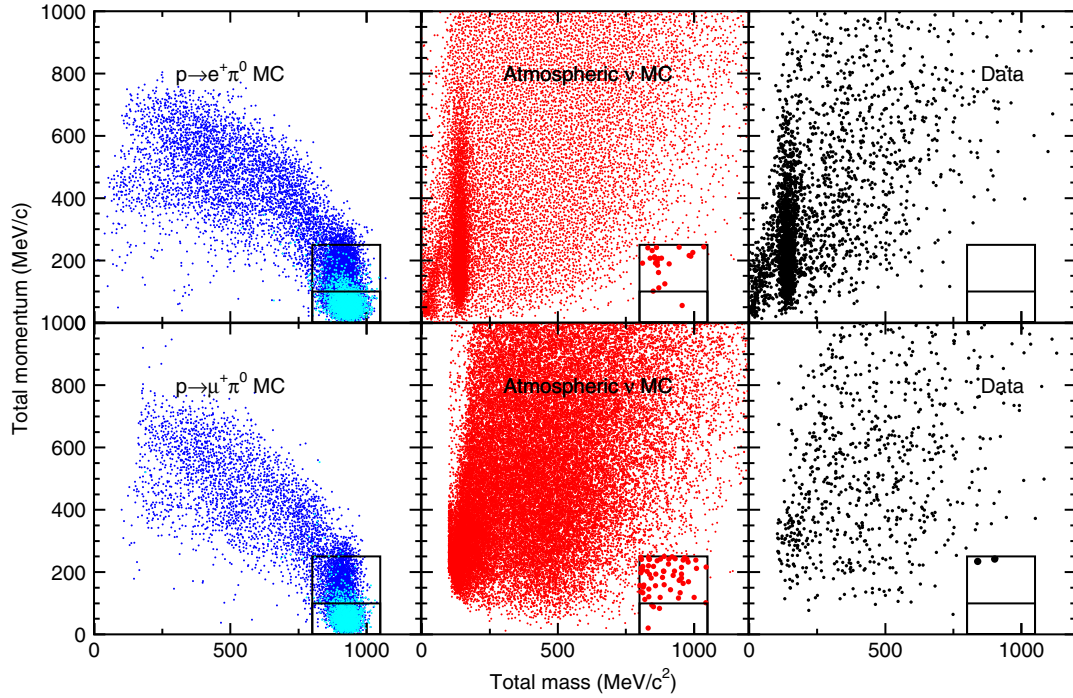


FIG. 3. Reconstructed proton mass vs total momentum for $p \rightarrow e^+ \pi^0$ (top) and $p \rightarrow \mu^+ \pi^0$ (bottom) after all cuts except (Cut-6). The left panels show signal MC, where light blue corresponds to free protons and dark blue is bound protons. The middle panels show atmospheric ν MC corresponding to 500 years live time of SK, and the right panels show SK-I to SK-IV data which contain 3408 and 1180 events for $p \rightarrow e^+ \pi^0$ and $p \rightarrow \mu^+ \pi^0$, respectively. The dot size is enlarged in the signal box.

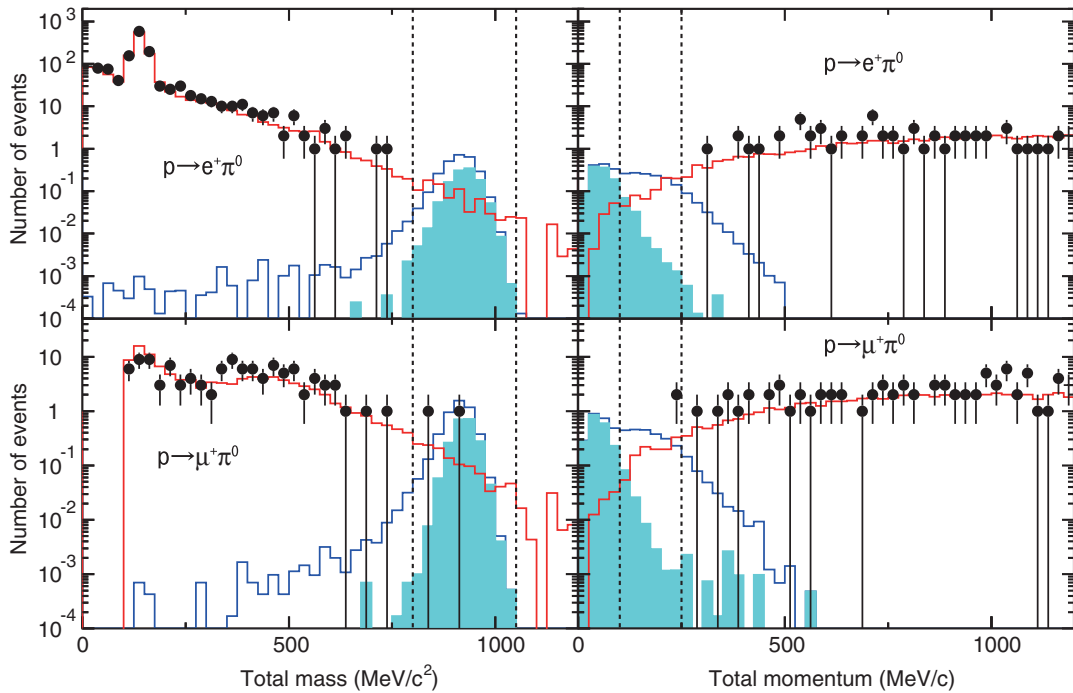


FIG. 4. Distributions of reconstructed invariant mass (left) and total momentum (right) for $p \rightarrow e^+ \pi^0$ in the top panels and for $p \rightarrow \mu^+ \pi^0$ in the bottom panels, after all selection cuts except cuts on the plotted variable. The dark blue histograms correspond to 90% confidence level allowed signal and the histograms filled by light blue show the portion contributed by free proton decay. The red histograms show atmospheric ν MC, and the dots are data with 0.306 Mton \cdot years exposure. Vertical dashed lines indicate the signal regions. The peak around 150 MeV/c^2 in the total mass distribution of atmospheric ν and data in the left top panel arises from π^0 decays.

by free protons, and the region $100 \leq P_{\text{tot}} < 250$ MeV/ c is dominated by bound protons. A reduced systematic error for < 100 MeV/ c can be achieved because the initial protons and the products of the proton decay do not suffer from any of the various nuclear interactions. In addition, background contamination from atmospheric neutrinos is concentrated in the $100 \leq P_{\text{tot}} < 250$ MeV/ c , while the region below 100 MeV/ c is nearly background free. Figure 3 shows the reconstructed proton mass vs total momentum distribution for signal and atmospheric ν MC, combining all data from SK-I through SK-IV. In the signal MC plots, the light blue dots show the free proton case and the dark blue dots show bound protons. Figure 4 shows one-dimensional distributions of reconstructed proton mass and momentum of $p \rightarrow e^+\pi^0$ and $p \rightarrow \mu^+\pi^0$ for the signal, atmospheric ν MC, and data after all cuts except the cut on the plotted variable. The data and the atmospheric ν MC agree in both cases.

The new two-box analysis achieves better discovery reach. For example, the 3σ discovery reach in the proton lifetime for $p \rightarrow e^+\pi^0$ is 13.3% higher than the conventional single-box analysis for the current exposure, and 20.9% higher for an exposure of 1 megaton \cdot year, which may be achieved by the next generation of detectors [30].

VI. RESULTS

Table I shows efficiency, expected number of background events, and number of observed events for each region of total momentum for $p \rightarrow e^+\pi^0$ and $p \rightarrow \mu^+\pi^0$. The signal efficiencies in SK-I and -II are decreased in comparison to the previous paper due to the updated π -FSI model. Efficiencies for $p \rightarrow \mu^+\pi^0$ in SK-IV are significantly higher than the other data-taking periods because of Michel electron tagging efficiency that was achieved with the new electronics. The background rate in SK-I/II/III is consistent with the measurement in the 1 kton water Cherenkov detector using the K2K accelerator neutrino beam [31]. Background rates in SK-IV for both decay modes are almost half that of SK-I/II/III, which is a result of the contribution from neutron tagging. In the entire signal region, with 306.3 kiloton \cdot years exposure, the expected background for $p \rightarrow e^+\pi^0$ is 0.61 events (0.07 and 0.54 events in lower and higher momentum box, respectively) and no candidates were observed, while for $p \rightarrow \mu^+\pi^0$ the estimated background is 0.87 events (0.05 and 0.82 events in lower and higher momentum box, respectively) and two candidates have been observed in the higher momentum box. Assuming a Poisson distribution with mean 0.87, the

TABLE I. Summary of the $p \rightarrow e^+\pi^0$ and $p \rightarrow \mu^+\pi^0$ proton decay modes. The selection efficiencies and expected backgrounds with quadratic sum of statistical and systematic errors, and number of observed events are shown for each detector period. Low P_{tot} and high P_{tot} are defined as $P_{\text{tot}} < 100$ MeV/ c and $100 \leq P_{\text{tot}} < 250$ MeV/ c , respectively.

		SK-I	SK-II	SK-III	SK-IV
Exp.	kt \cdot yrs	91.7	49.2	31.9	133.5
$p \rightarrow e^+\pi^0$					
Low P_{tot}	Eff.(%)	18.8 ± 1.9	18.3 ± 1.9	19.6 ± 2.0	18.7 ± 1.9
	BKG	$0.03^{+0.03}_{-0.02}$	< 0.01	< 0.01	$0.02^{+0.03}_{-0.02}$
	(/Mt \cdot yr)	$0.36^{+0.30}_{-0.20}$	$0.26^{+0.27}_{-0.17}$	$0.09^{+0.21}_{-0.08}$	$0.18^{+0.25}_{-0.13}$
	OBS	0	0	0	0
High P_{tot}	Eff.(%)	20.4 ± 3.6	20.2 ± 3.6	20.5 ± 3.6	19.4 ± 3.4
	BKG	0.22 ± 0.08	0.12 ± 0.04	0.06 ± 0.02	0.15 ± 0.06
	(/Mt \cdot yr)	2.4 ± 0.8	2.5 ± 0.9	1.8 ± 0.7	1.1 ± 0.3
	OBS	0	0	0	0
$p \rightarrow \mu^+\pi^0$					
Low P_{tot}	Eff.(%)	16.4 ± 1.5	16.0 ± 1.5	16.4 ± 1.5	20.1 ± 1.9
	BKG	$0.03^{+0.02}_{-0.02}$	< 0.01	< 0.01	$0.01^{+0.02}_{-0.01}$
	(/Mt \cdot yr)	$0.31^{+0.26}_{-0.17}$	$0.10^{+0.13}_{-0.07}$	$0.22^{+0.22}_{-0.14}$	$0.09^{+0.21}_{-0.08}$
	OBS	0	0	0	0
High P_{tot}	Eff.(%)	15.3 ± 2.8	15.3 ± 2.8	16.5 ± 3.0	18.2 ± 3.3
	BKG	0.33 ± 0.10	0.14 ± 0.05	0.12 ± 0.04	0.23 ± 0.08
	(/Mt \cdot yr)	3.6 ± 1.1	2.9 ± 0.9	3.7 ± 1.2	1.7 ± 0.6
	OBS	0	0	0	2

TABLE II. Summary of systematic errors for efficiencies, backgrounds, and exposures in percent (%). Low P_{tot} and high P_{tot} are defined as $P_{\text{tot}} < 100$ MeV/ c and $100 \leq P_{\text{tot}} < 250$ MeV/ c , respectively. For SK-IV only, a neutron tagging uncertainty is included, and the total systematic error for SK-IV is also shown including this uncertainty, both in parentheses.

		$p \rightarrow e^+ \pi^0$		$p \rightarrow \mu^+ \pi^0$	
		low P_{tot}	high P_{tot}	low P_{tot}	high P_{tot}
Efficiency	π -FSI	2.8	10.6	2.9	12.1
	Correlated decay	1.9	9.1	1.7	9.0
	Fermi momentum	8.5	9.3	8.0	9.6
	Reconstruction	4.6	5.6	3.7	3.3
	Total	10.2	17.7	9.4	18.2
Background	Flux	7.0	6.9	7.0	7.0
	Cross section	14.5	10.4	8.4	7.8
	π -FSI	15.4	15.4	14.2	14.4
	Reconstruction	21.7	21.7	21.7	21.7
	(neutron tag)	10	10	10	10
	Total (I/II/III)	31.2	29.4	28.1	28.1
	(IV)	32.7	31.1	29.9	29.8
Exposure		1.0	1.0	1.0	1.0

probability to see ≥ 2 events is 22% and is still consistent with background. The first candidate was observed at 257 kton · years exposure and the second candidate was observed at 277 kton · years exposure. A Kolmogorov-Smirnov test is carried out to examine the assumption of a constant event rate. The obtained p-value is 5.2%, which is consistent with the assumption.

Table II shows a summary of the systematic errors. The dominant systematic uncertainty in the efficiency of both decay modes in the $P_{\text{tot}} < 100$ MeV/ c region comes from uncertainty in the Fermi momentum. In the proton decay MC, the momentum distribution of the bound nucleon is simulated based on experimental data [32], which is compared with the Fermi gas model to estimate the uncertainty. Uncertainties in energy scale, uniformity of the detector, particle identification, vertex shift, opening angle, and ring counting are all taken into account as reconstruction error. Uncertainties in the $100 \leq P_{\text{tot}} < 250$ MeV/ c region are generally larger because they are mostly bound protons that suffer from uncertainties associated with π -FSI, correlated decays with other nucleons [33], and Fermi motion. The leading uncertainties in the background estimate come from cross section, π -FSI, and reconstruction. An additional systematic error for neutron tagging is assigned only for SK-IV. As shown in Fig. 2 and Ref. [18], neutron multiplicity in atmospheric neutrino data and MC agree well. Also, as described in Sec. III, the data with neutron source is compared with MC in several detector positions. The systematic error on neutron tagging is assigned to be 10% estimated by the maximum deviation between data and MC. The run time of SK is well defined and systematic uncertainty in the exposure is negligibly small (1%).

Both of the observed candidates for $p \rightarrow \mu^+ \pi^0$ are located near the boundary of the signal region. The first candidate has a reconstructed proton mass of 903 ± 19 MeV/ c^2 and 248 ± 5 MeV/ c total momentum. The first candidate is categorized as a 2-ring event; the e -like ring has momentum 375 MeV/ c , the μ -like ring has 551 MeV/ c momentum, and there is a 158° opening angle between the two rings. For the second candidate, the ring counting algorithm originally found one μ -like ring and two e -like rings. However, one of the e -like rings (orange ring in Fig. 5) is judged as a fake ring at the final stage of ring counting. This final stage discards rings caused by multiple Coulomb scattering of charged particles, which is done by examination of a ring's angle relative to other rings and by visible energy; it is applied to both data and MC. As a result, the second candidate is judged as a 2-ring event. In the final result of the reconstruction, the second candidate has a reconstructed proton mass of 832 ± 17 MeV/ c^2 and a total momentum of 238 ± 5 MeV/ c calculated from the remaining e -like ring with 461 MeV/ c , the μ -like ring with 391 MeV/ c , and the 149° angle between the two rings. If the third ring had not been rejected, the reconstructed invariant mass from the two e -like rings would have been 104 MeV/ c^2 , which could be gammas from π^0 decay. The total momentum and proton mass would increase to 289 MeV/ c and 880 MeV/ c^2 , respectively, which would move the event outside of the defined signal region.¹

¹This event is judged as a 3-ring event, but leaves the signal box if we use updated PMT gain correction, introduced in 2016, which depends on PMT production year.

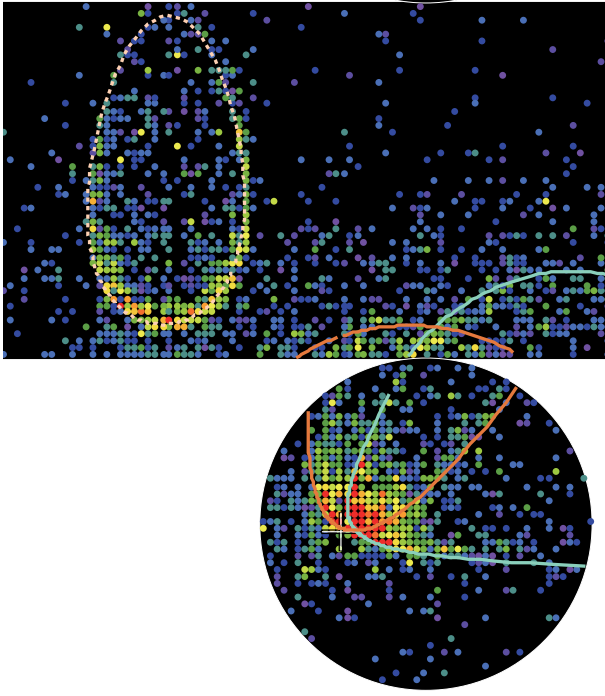


FIG. 5. Event display of the second candidate event, zoomed to the region of the rings. The blue solid line and the tan dashed line show the reconstructed e -like and μ -like rings, respectively. The dark orange solid line shows an additional e -like ring that was identified in the initial ring counting process, but it is rejected by the ring correction because it is too close in angle to the other e -like ring (blue line). As a result, this event is judged as a two-ring event.

VII. LIFETIME LIMIT

The observed events are consistent with expected backgrounds and a proton lifetime limit is calculated using a Bayesian method [34,35]. In Ref. [23], the proton lifetime was calculated combining different search methods as well as different run periods. The same method is used here for combining $P_{\text{tot}} < 100$ MeV/ c and $100 \leq P_{\text{tot}} < 250$ MeV/ c . For measurements $i = 1-4$ ($P_{\text{tot}} < 100$ MeV/ c , SK-I-SK-IV) and $5-8$ ($100 \leq P_{\text{tot}} < 250$ MeV/ c , SK-I-SK-IV), the conditional probability distribution for the decay rate is expressed as

$$P(\Gamma|n_i) = \iiint \frac{e^{-(\Gamma\lambda_i\epsilon_i + b_i)} (\Gamma\lambda_i\epsilon_i + b_i)^{n_i}}{n_i!} \times P(\Gamma)P(\lambda_i)P(\epsilon_i)P(b_i)d\lambda_i d\epsilon_i db_i \quad (1)$$

where n_i is the number of candidate events in the i th proton decay search, λ_i is the true detector exposure, ϵ_i is the true detection efficiency, and b_i is the true number of background events. The decay rate prior probability distribution $P(\Gamma)$ is 1 for $\Gamma \geq 0$ and otherwise 0. $P(\lambda_i)$, $P(\epsilon_i)$, and $P(b_i)$ are the prior probability distributions for detector exposure, efficiency, and background, respectively, which are assumed to be Gaussian distributions with σ described

in Table II [23]. The lower limit of the nucleon decay rate, Γ_{limit} , is

$$\text{C.L.} = \frac{\int_{\Gamma=0}^{\Gamma_{\text{limit}}} \prod_{i=1}^{N=8} P(\Gamma|n_i) d\Gamma}{\int_{\Gamma=0}^{\infty} \prod_{i=1}^{N=8} P(\Gamma|n_i) d\Gamma}, \quad (2)$$

where C.L. is the confidence level, taken to be 90%. The lower lifetime limit of $p \rightarrow l^+ \pi^0$ (l^+ denotes e^+ or μ^+) is given by

$$\tau/B_{p \rightarrow l^+ \pi^0} = \frac{1}{\Gamma_{\text{limit}}}. \quad (3)$$

The results of the limit calculation combining the two regions are

$$\tau/B_{p \rightarrow e^+ \pi^0} > 1.6 \times 10^{34} \text{ yr}, \quad \tau/B_{p \rightarrow \mu^+ \pi^0} > 7.7 \times 10^{33} \text{ yr},$$

at the 90% confidence level. $\tau/B_{p \rightarrow \mu^+ \pi^0}$ is lower than $\tau/B_{p \rightarrow e^+ \pi^0}$, and this is also lower than our previous publication [9] because of the two observed events, which are consistent with atmospheric neutrino background.

VIII. CONCLUSION

We analyzed 0.306 megaton \cdot years of Super-Kamiokande data to search for proton decay via $p \rightarrow e^+ \pi^0$ and $p \rightarrow \mu^+ \pi^0$. Neutron tagging was introduced in SK-IV and it succeeds in rejecting half of the backgrounds. The signal region from SK-I to SK-IV was divided into two regions of P_{tot} to obtain better sensitivity. We observed zero events (0.07 and 0.54 expected background in lower and higher momentum box, respectively) for $p \rightarrow e^+ \pi^0$ and two events in the higher momentum box (0.05, and 0.82 expected background in lower and higher momentum box, respectively) for $p \rightarrow \mu^+ \pi^0$. The obtained proton lifetime limits at 90% confidence level are $> 1.6 \times 10^{34}$ yr for $p \rightarrow e^+ \pi^0$ and $> 7.7 \times 10^{33}$ yr for $p \rightarrow \mu^+ \pi^0$.

ACKNOWLEDGMENTS

We gratefully acknowledge the cooperation of the Kamioka Mining and Smelting Company. The Super-Kamiokande experiment has been built and operated from funding by the Japanese Ministry of Education, Culture, Sports, Science and Technology, the U.S. Department of Energy, and the U.S. National Science Foundation. Some of us have been supported by funds from the National Research Foundation of Korea NRF-2009-0083526 (KNRC) funded by the Ministry of Science, ICT, and Future Planning, the European Union H2020 RISE-GA641540-SKPLUS), the Japan Society for the Promotion of Science, the National Natural Science Foundation of China under Grant No. 11235006, the National Science and Engineering Research Council (NSERC) of Canada, and the Scinet and Westgrid consortia of Compute Canada.

- [1] J. C. Pati and A. Salam, Unified lepton-hadron symmetry and a gauge theory of the basic interactions, *Phys. Rev. D* **8**, 1240 (1973); Is Baryon Number Conserved?, *Phys. Rev. Lett.* **31**, 661 (1973); H. Georgi and S. L. Glashow, Unity of All Elementary Particle Forces, *Phys. Rev. Lett.* **32**, 438 (1974).
- [2] K. S. Babu, E. Kearns *et al.*, Working Group Report: Baryon Number Violation, [arXiv:1311.5285](https://arxiv.org/abs/1311.5285).
- [3] J. R. Ellis, D. V. Nanopoulos, and J. Walker, Flipping SU(5) out of trouble, *Phys. Lett. B* **550**, 99 (2002).
- [4] P. Langacker, Grand unification and the standard model, [arXiv:hep-ph/9411247](https://arxiv.org/abs/hep-ph/9411247).
- [5] C. McGrew *et al.* (IMB Collaboration), Search for nucleon decay using the IMB-3 detector, *Phys. Rev. D* **59**, 052004 (1999).
- [6] K. S. Hirata *et al.* (Kamiokande Collaboration), Experimental limits on nucleon lifetime for lepton + meson decay modes, *Phys. Lett. B* **220**, 308 (1989).
- [7] M. Shiozawa *et al.* (Super-Kamiokande Collaboration), Search for Proton Decay via $p \rightarrow e^+ \pi^0$ in a Large Water Cherenkov Detector, *Phys. Rev. Lett.* **81**, 3319 (1998).
- [8] H. Nishino *et al.* (Super-Kamiokande Collaboration), Search for Proton Decay via $p \rightarrow e^+ \pi^0$ and $p \rightarrow \mu^+ \pi^0$ in a Large Water Cherenkov Detector, *Phys. Rev. Lett.* **102**, 141801 (2009).
- [9] H. Nishino *et al.* (Super-Kamiokande Collaboration), Search for nucleon decay into charged antilepton plus meson in Super-Kamiokande I and II, *Phys. Rev. D* **85**, 112001 (2012).
- [10] J. Hisano, H. Murayama, and T. Yanagida, Nucleon decay in the minimal supersymmetric SU(5) grand unification, *Nucl. Phys. B* **402**, 46 (1993); H. Murayama and A. Pierce, Not even decoupling can save minimal supersymmetric SU(5), *Phys. Rev. D* **65**, 055009 (2002).
- [11] K. S. Babu and S. Khan, Minimal nonsupersymmetric SO(10) model: Gauge coupling unification, proton decay, and fermion masses, *Phys. Rev. D* **92**, 075018 (2015); G. Altarelli and D. Meloni, A nonsupersymmetric SO(10) grand unified model for all the physics below M_{GUT} , *J. High Energy Phys.* **08** (2013) 021.
- [12] G. Aad *et al.* (ATLAS and CMS Collaborations), Combined Measurement of the Higgs Boson Mass in pp Collisions at $\sqrt{s} = 7$ and 8 TeV with the ATLAS and CMS Experiments, *Phys. Rev. Lett.* **114**, 191803 (2015).
- [13] J. Hisano, D. Kobayashi, T. Kuwahara, and N. Nagata, Decoupling can revive minimal supersymmetric SU(5), *J. High Energy Phys.* **07** (2013) 038; H. Fukuda, H. Murayama, T. Yanagida, and N. Yokozaki, Semirational gauge mediation from product group unification, *Phys. Rev. D* **92**, 055032 (2015).
- [14] Y. Fukuda *et al.* (Super-Kamiokande Collaboration), The Super-Kamiokande detector, *Nucl. Instrum. Methods Phys. Res., Sect. A* **501**, 418 (2003); K. Abe *et al.* (Super-Kamiokande Collaboration), Calibration of the Super-Kamiokande detector, *Nucl. Instrum. Methods Phys. Res., Sect. A* **737**, 253 (2014).
- [15] H. Nishino, K. Awai, Y. Hayato, S. Nakayama, K. Okumura, M. Shiozawa, A. Takeda, K. Ishikawa, A. Minegishi, and Y. Arai, High-speed charge-to-time converter ASIC for the Super-Kamiokande detector, *Nucl. Instrum. Methods Phys. Res., Sect. A* **610**, 710 (2009); S. Yamada *et al.* (Super-Kamiokande Collaboration), Commissioning of the new electronics and online system for the Super-Kamiokande experiment, *IEEE Trans. Nucl. Sci.* **57**, 428 (2010).
- [16] H. Zhang *et al.* (Super-Kamiokande Collaboration), Supernova relic neutrino search with neutron tagging at Super-Kamiokande-IV, *Astropart. Phys.* **60**, 41 (2015).
- [17] Y. Zhang *et al.* (Super-Kamiokande Collaboration), First measurement of radioactive isotope production through cosmic-ray muon spallation in Super-Kamiokande IV, *Phys. Rev. D* **93**, 012004 (2016).
- [18] T. J. Irvine, Ph.D. thesis, University of Tokyo, 2014.
- [19] Y. Hayato, NEUT, *Nucl. Phys. B, Proc. Suppl.* **112**, 171 (2002); G. Mitsuka, NEUT, *AIP Conf. Proc.* **967**, 208 (2007); *AIP Conf. Proc.* **981**, 262 (2008).
- [20] M. Honda, T. Kajita, K. Kasahara, and S. Midorikawa, Improvement of low energy atmospheric neutrino flux calculation using the JAM nuclear interaction model, *Phys. Rev. D* **83**, 123001 (2011).
- [21] H. W. Bertini, Intranuclear-cascade calculation of the secondary nucleon spectra from nucleon-nucleus interactions in the energy range 340 to 2900 MeV and comparisons with experiment, *Phys. Rev.* **188**, 1711 (1969).
- [22] J. O. Johnson and T. A. Gabriel, Report No. ORNL/TM-10340, 1988.
- [23] K. Abe *et al.* (Super-Kamiokande Collaboration), Search for proton decay via $p \rightarrow \nu K^+$ using 260 kiloton year data of Super-Kamiokande, *Phys. Rev. D* **90**, 072005 (2014).
- [24] H. Ejiri, Nuclear deexcitations of nucleon holes associated with nucleon decays in nuclei, *Phys. Rev. C* **48**, 1442 (1993).
- [25] K. Abe *et al.* (T2K Collaboration), Evidence of electron neutrino appearance in a muon neutrino beam, *Phys. Rev. D* **88**, 032002 (2013).
- [26] R. A. Giannelli *et al.*, Multiproton final states in positive pion absorption below the Delta (1232) resonance, *Phys. Rev. C* **61**, 054615 (2000); A. Saunders, S. Hoibraten, J. J. Kraushaar, B. J. Kriss, R. J. Peterson, R. A. Ristinen, J. T. Brack, G. Hofman, E. F. Gibson, and C. L. Morris, Reaction and total cross-sections for low-energy π^+ and π^- on isospin zero nuclei, *Phys. Rev. C* **53**, 1745 (1996); I. Navon, D. Ashery, J. Alster, G. Azuelos, B. M. Barnett, W. Gyles, R. R. Johnson, D. R. Gill, and T. G. Masterson, True absorption and scattering of 50-MeV pions, *Phys. Rev. C* **28**, 2548 (1983); T. J. Bowles *et al.*, Inclusive (π^\pm , π^0) reactions in nuclei, *Phys. Rev. C* **23**, 439 (1981); D. Ashery, I. Navon, G. Azuelos, H. K. Walter, H. J. Pfeiffer, and F. W. Schlegel, True absorption and scattering of pions on nuclei, *Phys. Rev. C* **23**, 2173 (1981); D. Ashery *et al.*, Inclusive pion single charge exchange reactions, *Phys. Rev. C* **30**, 946 (1984); S. M. Levenson *et al.*, Inclusive pion scattering in the Delta (1232) region, *Phys. Rev. C* **28**, 326 (1983); M. K. Jones *et al.*, Pion absorption above the Delta (1232) resonance, *Phys. Rev. C* **48**, 2800 (1993); P. Chavanon, M. Crozon, T. Leray, and J. Tocqueville, Determination of the pion neutral angular distribution in the reaction π^+ , $p \rightarrow \pi^+$, p , π^0 in the energy range 600 to 1300 MeV (in French), *Phys. Lett. B* **28**, 296 (1968); T. Takahashi *et al.*, π^- - ^{12}C elastic scattering above the Δ

- resonance, *Phys. Rev. C* **51**, 2542 (1995); B. W. Allardyce *et al.*, Pion reaction cross-sections and nuclear sizes, *Nucl. Phys. A* **209**, 1 (1973); J. W. Cronin, R. Cool, and A. Abashian, Cross sections of nuclei for high-energy pions, *Phys. Rev.* **107**, 1121 (1957); K. Aoki *et al.*, Elastic and inelastic scattering of π^+ and π^- on C12 at 995 MeV/c, *Phys. Rev. C* **76**, 024610 (2007); A. Rahav *et al.*, Measurement of the C-12(π ,2 π) reactions and possible evidence of a double Delta excitation, *Phys. Rev. Lett.* **66**, 1279 (1991).
- [27] K. Abe *et al.* (Super-Kamiokande Collaboration), Search for Nucleon Decay via $n \rightarrow \bar{\nu}\pi^0$ and $p \rightarrow \bar{\nu}\pi^+$ in Super-Kamiokande, *Phys. Rev. Lett.* **113**, 121802 (2014).
- [28] J. F. Beacom and M. R. Vagins, Antineutrino Spectroscopy with Large Water Čerenkov Detectors, *Phys. Rev. Lett.* **93**, 171101 (2004).
- [29] K. Nakamura and M. Shiozawa, in *Proceedings of the 2nd International Workshop on Neutrino Oscillations and Their Origin (NOON 2000)*, Tokyo, Japan, 2000, edited by Y. Suzuki *et al.* (World Scientific, Singapore, 2001), pp. 276–287.
- [30] K. Abe *et al.*, Letter of Intent: The Hyper-Kamiokande Experiment—detector design and physics potential, [arXiv: 1109.3262](https://arxiv.org/abs/1109.3262).
- [31] S. Mine *et al.* (K2K Collaboration), Experimental study of the atmospheric neutrino backgrounds for $p \rightarrow e^+\pi^0$ searches in water Cherenkov detectors, *Phys. Rev. D* **77**, 032003 (2008).
- [32] K. Nakamura, S. Hiramatsu, T. Kamae, H. Muramatsu, N. Izutsu, and Y. Watase, The reaction $^{12}\text{C}(e, e'p)$ at 700 MeV and DWIA Analysis, *Nucl. Phys. A* **268**, 381 (1976).
- [33] T. Yamazaki and Y. Akaishi, Nuclear medium effects on invariant mass spectra of hadrons decaying in nuclei, *Phys. Lett. B* **453**, 1 (1999).
- [34] C. Amsler *et al.* (Particle Data Group Collaboration), Review of particle physics, *Phys. Lett. B* **667**, 1 (2008).
- [35] B. P. Roe and M. B. Woodroffe, Setting confidence belts, *Phys. Rev. D* **63**, 013009 (2000).